Single-Molecule Spectroscopic Study of Enhanced Intrinsic Phycoerythrin Fluorescence on Silver Nanostructured Surfaces

Krishanu Ray,* Mustafa H. Chowdhury, and Joseph R. Lakowicz

Center for Fluorescence Spectroscopy, Department of Biochemistry and Molecular Biology, University Maryland School of Medicine, 725 West Lombard Street, Baltimore, Maryland 21201

In this paper, we report on steady-state and time-resolved single-molecule fluorescence measurements performed on a phycobiliprotein, R-phycoerythrin (RPE), assembled on silver nanostructures. Single-molecule measurements clearly show that RPE molecules display a 10-fold increase in fluorescence intensity, with a 7-fold decrease in lifetime when they are assembled on silver nanostructured surfaces, as compared to control glass slides. The emission spectrum of individual RPE molecules also displays a significant fluorescence enhancement on silver nanostructures as compared to glass. From intensity and lifetime histograms, it is clear that the intensities as well as lifetimes of individual RPE molecules on silver nanostructures are more heterogeneously distributed than that on glass. This single-molecule study provides further insight on the heterogeneity in the fluorescence intensity and lifetimes of the RPE molecules on both glass and SiFs surfaces, which is otherwise not possible to observe using ensemble measurements. Finite-difference time-domain calculations have been performed to study the enhanced near-fields induced around silver nanoparticles by a radiating excited-state fluorophore, and the effect of such enhanced fields on the fluorescence enhancement observed is discussed.

Phycobiliproteins, unique photosynthetic pigment–protein complexes, play a crucial role in harvesting sunlight that chlorophylls poorly absorb and then transfering this energy via various energy-transfer mechanisms to chlroophyll in the membranes of these organisms.[1–4] Phycobiliproteins possess several unique characteristics that make them attractive for use as fluorescence labels in the analysis of biomolecules and cells. Some of the desirable properties of phycobiliproteins include high absorbance coefficients over a wide region of the visible spectra, high fluorescence quantum yields that are constant over a broad pH range, large Stokes shift that minimizes interferences from Rayleigh and Raman scatter and other autofluorescing species,

and strong emission bands that extend well into the red region of the visible spectrum where there is minimal interference from biological molecules.[1–8] The fluorescent protein phycoerythrin has a very high extinction coefficient and large Stokes shift. We selected R-phycoerythrin (RPE), which is a 240-kDa autofluorescent protein consisting of 7 subunits and 30 chromophores.[4,9] Phycobiliproteins such as RPE are stable and highly water-soluble globular proteins derived from cyanobacteria and eukaryotic algae. Phycobiliproteins are of interest because they can be 10–100-fold brighter than organic fluorophores. Remarkably, we found that they can be made even brighter by bringing them in proximity to silver nanoparticles.

Single-molecule detection (SMD) is a powerful tool to study the properties of individual fluorophores and the dynamics of biomolecules.[10–13] SMD is valuable because the measurements bypass the ensemble averaging that occurs in traditional fluorescence measurements. Fluorophores primarily chosen for single-molecule measurements include fluorescent organic dye molecules, quantum dots, and fluorescent proteins. The fluorophores for SMD must be bright (quantum yield >0.1) with high extinction coefficient, photostable, short excited-state lifetime, and large Stokes' shift. A high extinction coefficient is needed to maximize the absorption cross section of the fluorophore. A short excited-state lifetime is needed to allow the fluorophore to cycle rapidly between the ground and excited states and thus have a high emission rate. In order to observe single fluorophores, the incident intensities must be high to obtain high rates of excitation and emission. As a result, single fluorophores can be observed for only a short period of time, typically seconds, prior to photobleaching. Additionally, observation of single fluorophores is usually accomplished using diffraction-limited volumes. Otherwise the single-molecule emission is overwhelmed from the background due to autofluorescence or Raman scatter. The extinction coefficient, quantum yield, and lifetimes all contribute to the brightness of the fluorophore. A modest decrease in brightness

* To whom correspondence should be addressed. E-mail: krishanu@cfs.umbi.umd.edu.

(1) Oi, V. T.; Glazer, A. N.; Stryer, L. *J. Cell. Biol.* **1982**, *93*, 981.
(2) Glazer, A. N.; Stryer, L. *Biophys. J.* **1983**, *43*, 383–386.
(3) Gaigalas, A.; Gallagher, T.; Cole, K. D.; Singh, T.; Wang, L.; Zhang, Y. *Photochem. Photobiol.* **2006**, *82*, 635.
(4) Lakowicz, J. R. *Principles of Fluorescence Spectroscopy*; Springer: New York, 2006; Chapter 3.

(5) Kronick, M. N.; Grossman, P. D. *Clin. Chem.* **1983**, *29*, 1582.
(6) Kang, S.; Yeung, E. S. *Anal. Chem.* **2002**, *74*, 6334.
(7) Wellman, A.; Sepaniak, M. J. *Anal. Chem.* **2006**, *78*, 4450.
(8) Guard-Friar, D.; MacColl, R.; Berns, D. S.; Wittmershaus, B.; Knox, R. S. *Biophys. J.* **1985**, *47*, 787.
(9) Goulian, M.; Simon, S. M. *Biophys. J.* **2000**, *79*, 2188.
(10) Michalet, X.; Weiss, S.; Jager, M. *Chem. Rev.* **2006**, *106*, 1785.
(11) Rigler, R.; Orrit, M.; Basche, T. *Single Molecule Spectroscopy*; Springer: New York, 2001.
(12) Cornis, P. V.; Ha, T. *ACS Chem. Biol.* **2007**, *2*, 53.
(13) Moerner, W. E. *J. Phys. Chem. B* **2002**, *106*, 910.

makes a fluorophore not useful for single-molecule studies. The use of fluorophore−metal interactions has the potential to significantly increase the brightness or detectability of single fluorophores. SMD is a valuable tool for studying fluorophore−metal interactions. This is because the substrates commonly used in fluorophore−metal interactions are heterogeneous in nature such as silver island films (SiFs) and thin films of metal thermally evaporated on glass slides. For such structures, the nature of the individual fluorophore−metal interactions depends heavily on the location of a particular fluorophore with respect to the nearest metal structures. Hence, with SMD, we can specifically study such individual interactions. In ensemble measurements, such subtle differences are not observed as the signal obtained is averaged over the entire observation region. In the case of fluorophores coated on ordered metallic structures such as nanoparticle arrays of different shapes, the individual fluorophores can be located in a myriad of locations on the array. Some can be on the tip of the metal structure, whereas others can be in the middle of a flat region of the metal nanostructures and others can be in between two metal nanoparticles. Hence, even for a ordered metallic structure, we can expect a heterogeneity in the mode of interaction of individual fluorophores with the metal nanostructures. As a result, SMD is useful to study the individual metal−fluorophore interactions.[14,15] We believe that SMD of phycobiliproteins on silver nanostructures is interesting as certain phenomena not necessarily predictable by ensemble experiments, such as fluctuations in the fluorescence intensity, lifetime, or emission maximum, can be detected by SMD. The fluorescent protein phycoerythrin was the first molecule to be observed at the single-molecule level using laser-induced fluorescence.[16,17] Phycobiliproteins have also been the focus of several single-molecule spectroscopy studies and also have been used in high-speed, high-throughput, single-molecule imaging techniques for identifying in free solution biomolecules—a technique with potential for use in high-speed detection of specific disease markers.[18−21] Hence, further enhancing the fluorescence emission properties and improving the photostability of phycobiliproteins will serve to make them even more efficient labels in the analysis of biomolecules and cells. One way of doing this is via the interaction of the phycobiliproteins with silver nanostructures to achieve metal-enhanced fluorescence (MEF), which can be used to increase the photostability, brightness, and increase in radiative decay rates of fluorophores.[14,15] Phycobiliproteins are large intrinsically fluorescent protein molecules with multiple chromophores. This is unlike small organic dyes, which have only one chromophore. Although our laboratory have published numerous papers on MEF with various organic dyes and quantum dots,[14,15,22−29] there are only few MEF results reported in the literature that deal with intrinsically fluorescent proteins. In this respect, ensemble fluorescence spectroscopic studies show that the emission of intrinsically fluorescent proteins also can be significantly enhanced by silver nanostructures,[29] which can be useful in sensing applications.

Here we report on single-molecule fluorescence experiments performed on phycobiliproteins assembled on silver nanostructures. Our single-molecule measurements show that the phycobiliproteins display an appreciable increase in fluorescence emission intensity and decrease in lifetime when they were assembled on the silver nanostructured surfaces as compared to glass substrates. This effect is due to the close-range (within 100 nm) interactions of these proteins with plasmonic nanoparticles. Hence, this study strongly suggests that MEF can be employed to increase the sensitivity and detection limit of the plethora of bioassays that employ phycobiliproteins as fluorescence labels. To the best of our knowledge, this is the first report demonstrating metal-enhanced fluorescence at the single-molecule level from biological macromolecules such as phycobiliproteins.

We also used the finite-difference time-domain (FDTD) computational technique to explain our experimental results. FDTD is an implementation of Maxwell's time-dependent curl equations for solving the temporal variation of electromagnetic waves within a finite space that contains a target of arbitrary shape.[30−37] In recent years, FDTD has become the state-of-the-art method for solving Maxwell's equations for complex geometries and offers the user a unique insight into many photonics-related problems.[30−37] Additional information on the FDTD technique can be found in refs 30–37. Our calculations reveal that excited-state fluorophores in the near-field of a silver nanoparticle induce enhancements of the near-fields around the particle, which we believe play a role in the experimental observations of MEF from the SiF substrates that is reported here.

EXPERIMENTAL SECTION

SiFs on cover glass slides were prepared as described previously.[23] A portion of the SiF sample was cut and coated with a thin layer of gold (∼5 nm) in a sputter coating system. This step was done to minimize charging effects during scanning electron

(14) Lakowicz, J. R. *Anal. Biochem.* **2005**, *337*, 171.
(15) Ray, K.; Badugu, R.; Lakowicz, J. R. *J. Am. Chem. Soc.* **2006**, *128*, 8998.
(16) Nguyen, D. C.; Keller, R. A.; Jett, J. H.; Martin, J. C. *Anal. Chem.* **1987**, *59*, 2158.
(17) Peck, K.; Stryer, L.; Glazer, A. N.; Mathies, R. A. *Proc. Natl. Acad. Sci. U. S. A.* **1989**, *86*, 4087.
(18) Yeung, E. S. *Annu. Rev. Phys. Chem.* **2004**, *55*, 97.
(19) Wu, M.; Goodwin, P. M.; Ambrose, W. P.; Keller, R. A. *J. Phys. Chem.* **1996**, *100*, 17406.
(20) Ma, Y.; Shortreed, M. R.; Yeung, E. S. *Anal. Chem.* **2000**, *72*, 4640.
(21) Davey, L.; Cotlet, M.; De Schryver, F.; Habuchi, S.; Hofkens, J. *Biophys. J.* **2004**, *87*, 2598.
(22) Lakowicz, J. R.; Shen, Y.; Gryczynski, Z.; D'Auria, S.; Gryczynski, I. *Biochem. Biophys. Res. Commun.* **2001**, *286*, 875.
(23) Lakowicz, J. R.; Shen, Y.; D'Auria, S.; Malicka, J.; Fang, J.; Grcyzynski, Z.; Gryczynski, I. *Anal. Biochem.* **2002**, *301*, 261.
(24) Zhang, J.; Matveeva, E.; Gryczynski, I.; Leoneko, Z.; Lakowicz, J. R. *J. Phys. Chem. B* **2005**, *109*, 7969.
(25) Aslan, K.; Gryczynski, I.; Malicka, J.; Matveeva, E.; Lakowicz, J. R.; Geddes, C. D. *Curr. Opin. Biotechnol.* **2005**, *16*, 55.
(26) *Topics in Fluorescence Spectroscopy*; Geddes, C.D., Lakowicz, J. R., Eds.; Kluwer Academic/Plenum Publishers: New York, 2005; *Vol. 8*.
(27) Ray, K.; Badugu, R.; Lakowicz, J. R. *J. Phys. Chem. B* **2006**, *110*, 13499.
(28) Ray, K.; Chowdhury, M.; Lakowicz, J. R. *Anal. Chem.* **2007**, *79*, 6480.
(29) Chowdhury, M.; Ray, K.; Aslan, K.; Lakowicz, J. R.; Geddes, C. D. *J. Phys. Chem. C* **2007**, *111*, 18856.
(30) Taflove, A., Hagness, S. C. *Computational Electrodynamics: The Finite-Difference Time-Domain Method*; Artech House: Boston, 2000.
(31) Sullivan, D. M. *Electromagnetic simulation using the FDTD method*; IEEE Press: New York, 2000.
(32) Yang, P.; Liou, N. K. *J. Opt. Soc. Am. A* **1996**, *13*, 2072.
(33) Gray, S. K.; Kupka, T. *Phy. Rev. B.* **2003**, *68*, 045415.
(34) Chang, S. H.; Gray, S. K.; Schatz, G. C. *Opt. Express* **2005**, *13*, 3150.
(35) Taflove, A.; Brodwin, M. E. *IEEE Trans. Microwave Theory Tech.* **1975**, *23*, 623.
(36) Reference Guide for FDTD Solutions, Release 5.0, 2007; http://www.lumerical.com/fdtd.
(37) Chowdhury, M. H.; Gray, S. K.; Pond, J.; Geddes, C. D.; Aslan, K.; Lakowicz, J. R. *J. Opt. Soc. Am. B* **2007**, *24*, 2259.

microscope (SEM) imaging. The sample was then mounted on an Al stub with conductive tape and observed in a Hitachi SU-70 SEM. Due to the nonconductive substrate (glass), low voltage (3 kV) was employed for high-resolution shallow surface observation and imaging using beam deceleration technology. Samples were surveyed at low magnifications to see the general features and the homogeneity. Representative areas were selected for higher magnification investigation.

Glass cover slides or SiFs were covered with 250 μL of 10 μM biotinylated bovine serum albumin (BSA-biotin, Sigma) aqueous solution and placed in a humid chamber for 20 h (5 °C). Following this step, the slides were then washed 3 times with PBS buffer and were placed again in the humid chamber. After that, a 250-μL sample of 200 pM streptavidin conjugated RPE (Sigma) in 100 mM PBS buffer was then added to each BSA-biotin-coated surface for 2 h at 5 °C. The slides were then washed multiple times with PBS buffer. The resulting streptavidin−RPE monolayer on glass or SiF surfaces was used for fluorescence measurement. The immobilized protein was always kept in the wet condition while performing ensemble or single-molecule measurements to prevent protein unfolding or denaturization through drying. For ensemble measurements, the concentration of the incubating solution of streptavidin-conjugated RPE was ∼1 μM.

Ensemble emission spectra of probes on solid substrates were recorded using a Varian Cary Eclipse fluorescence spectrophotometer. Both the steady-state and time-domain lifetime measurements were carried out using front face illumination. Time-domain lifetime measurements were obtained on a Pico-Quant lifetime fluorescence spectrophotometer (Fluotime 100).

Observations of single-molecule fluorescence were made with a scanning confocal Picoquant MicroTime 200 microscope with time-correlated single-photon counting capabilities. The excitation laser was reflected by a dichroic mirror to a high numerical aperture (NA) oil objective (100×, NA 1.3) and focused to a diffraction-limited spot (∼300 nm) on the sample surface. The fluorescence from the phycobiliproteins was collected by a single-photon counting avalanche photodiode through the dichroic beam splitter and a band-pass (550−600 nm, Chroma) filter. Single-molecule fluorescence images were recorded by raster scanning the sample through the excitation light focus by means of a linearized piezoscanner. The samples were excited with a typical power density of 200 W/cm^2 from a 470-nm pulsed laser (20-MHz repetition rate, 80-ps fwhm). Intensity−time trajectories and intensity−time decays were obtained by positioning the excitation beam above the individual RPE. The arrival time of each photon (100-ns resolution) and the fluorescence delay time relative to the laser pulse (37-ps resolution) were recorded for each detection channel and stored for later analysis. We have extended the capabilities of the Microtime 200 to include single-molecule spectral imaging with the addition of a spectrograph and an electron-multiplied CCD. For spectroscopy of individual molecules, a 150-mm spectrograph (Princeton Instruments Acton) has been employed. The spectrograph consists of high-reflectance mirrors (used for collimation and focusing), and a 150 G/mm dispersion grating with 500-nm blaze wavelength; this grating provides efficient imaging from 450 to 750 nm. The detector for the spectrograph is a high quantum efficient (>90% visible range) electron-multiplied CCD (Princeton Instruments Photon Max 512).

These EM-CCDs are commonly used for single-molecule spectral imaging.

FDTD calculations were performed using the program FDTD Solutions (Version 5.0) purchased from Lumerical Solutions, Inc. (Vancouver, Canada). The calculations were performed with the parallel FDTD option on a Dell Precision PWS690 workstation with the following components: Dual Quad-Core Intel Xeon E5320 processors at 1.86 GHz and 8 GB RAM. All postprocessing of FDTD data was performed using MATLAB (version 7.0) purchased from Mathworks (Natick, MA). A time-windowed dipole source, radiating at a fixed wavelength of 570 nm, was used to mimic the emission of R-phycoerythrin. This is a soft source, to allow backscattered radiation to pass through it.[35,37] All of the calculations were done by assuming a background refractive index of 1.0. The auxiliary differential equations method[30,37] was used to implement a realistic, frequency-dependent, and lossy dielectric model for the silver nanoparticle. In order to maintain the accuracy and stability of the FDTD calculations, the smallest grid size to accurately model the prescribed system without being computationally prohibitive was obtained in an iterative fashion (convergence testing). After testing for convergence, we used a grid size of 1 nm in our calculations. The numerical implementation of Maxwell's equations in the FDTD algorithm requires that the time increment Δt have a specific bound relative to the spatial discretization Δ (as mentioned above) to ensure the stability of the time-stepping algorithm. Our typical simulations were ranged around 400 fs, which led to all of our simulations having an excess of 200 000 time steps. Our FDTD software has frequency-domain monitors that perform discrete Fourier transforms of the time-domain fields while the simulation is running. In this manner, continuous wave (CW) information is obtained at any prespecified wavelengths for the various field components (E_x, E_y, E_z, H_x, H_y, H_z). Additionally, the time-domain monitors can provide time-domain information for the various field components within the FDTD simulation region over the entire course of the simulation. At the end of the simulation, the various field components are checked to see if they decay to zero, thus indicating that the simulation has run for a sufficiently long time for the CW information obtained by Fourier transformations to be valid.[36,37]

RESULTS AND DISCUSSION

Figure 1 shows the electron micrographs of the SiF surfaces. From these micrographs, we observe the nanoscale heterogeneity of the particles' sizes, shapes, and spatial distributions and the average size of these particles is ∼100 nm.

Figure 2 shows the ensemble fluorescence emission spectra and corresponding intensity decays of streptavidin-conjugated RPE molecules assembled on biotinylated glass and SiF surfaces. A significant enhancement (∼10-fold) in fluorescence intensity and ∼3-fold decrease in average fluorescence lifetime were observed from the RPE molecules on the SiF surface as compared to that on the glass. Interestingly, the ensemble emission spectra of RPE from glass and SiF surfaces are completely overlapped on each other with a band maximum at ∼573 nm. The increase in fluorescence intensity and decrease in lifetime of RPE molecules near silver nanostructures are due to an enhanced local field and an increase in the intrinsic decay rate of the fluorophore, both due to MEF.
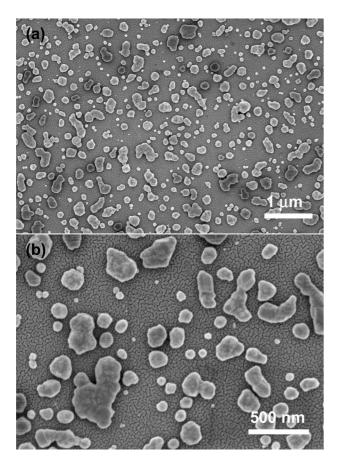
Figure 1. Field emission SEM images of SiFs on glass slides. Magnification (a) 20000× and (b) 50000×. Accelerating voltage of electron beam is 3 kV.

Figure 3 shows a representative 20 × 20 μm single-molecule images of RPE collected using confocal optics and stage scanning. Well-separated bright spots represent fluorescence emission from the individual RPE molecules. The significant differences in the peak intensities of the two images are immediately evident from Figure 3. The density of spots observed on glass (not shown) increases with higher incubation dye concentrations,which also confirms the observation of single RPE molecules. The intensities of the individual spots are considerably brighter on the SiFs than on glass.

To more quantitatively compare the collected single-molecule count rates and explore the changes in underlying photophysics of single RPE molecules on glass and SiF surfaces, we monitored the fluorescence intensity of individual RPE molecules as a function of time, while under continuous excitation. While observing the individual RPE molecules under continuous illumination, all the fluorophores display blinking. Examples of the blinking are shown in Figure 4a and b for five different RPE molecules. In each case,the intensity fluctuates dramatically, and eventually the emission stops when the molecule undergoes complete photodestruction. The intensity−time trajectories in Figure 4a and b are representative of the overall trend observed from more than 100 individual RPE molecules tethered to glass or SiF surfaces by the biotin−streptavidin chemistry. The spots on glass and on the SiF both showed single-step photobleaching, corresponding to the typical behavior expected for a single molecule (Figure 4a and b). Although the phycobiliproteins are multiple chromophore-based molecules, the single-step photobleaching shown in our
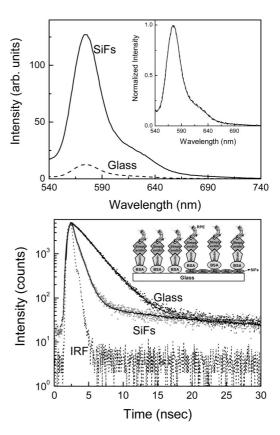

Figure 2. Top panel: Ensemble fluorescence spectra of streptavidin-conjugated RPE assembled on biotinylated glass and SiF surfaces. Inset shows the normalized emission spectra. Bottom panel: Intensity time decay of RPE on glass and SiF surface. Instrument response function (IRF) is also included. Inset shows the schematic representation of the sample configuration.
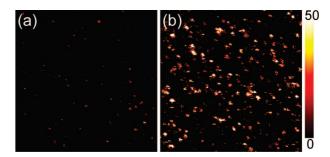

Figure 3. Scanning confocal images (20 × 20 μm) of RPE on (a) glass and (b) SiFs. Scale bar shows the intensity counts in 1-ms bin.

results indicate that the phycobiliproteins behave as single quantum events. This phenomenon was also observed by other groups.[18,19]

An important feature of SMD is the ability to examine the behavior of a single molecule rather than the average behavior of numerous molecules. This property could be revealed by recording the emission spectrum of an individual molecule.[38,39] Figure 5a presents representative spectra of individual RPE molecules on glass and SiF surfaces, respectively. Individual RPE molecules both on glass and SiF surfaces displayed spectra with unique properties. Often the single-molecule spectra are the same

(38) Weston, K. D.; Carson, P. J.; Meitu, H.; Burrato, S. K. *J. Chem. Phys.* **1998**, *109*, 7474.
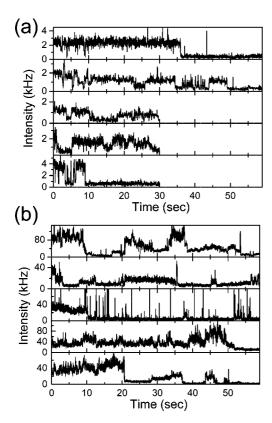(39) Moerner, W. E.; Fromm, D. P. *Rev. Sci. Instrum.* **2003**, *74*, 3597.

Figure 4. Intensity−time trajectories of individual RPE molecules on (a) glass and (b) SiF surfaces.
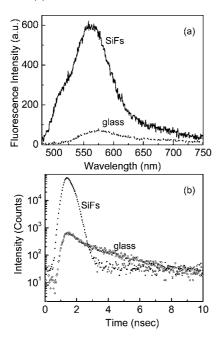

Figure 5. (a) Single-molecule fluorescence spectra of individual RPE on glass and SiFs surfaces. (b) Fluorescence intensity decays of individual RPE molecules on glass and SiF surfaces.

Figure 6. Fluorescence intensity (count rate) histogram of RPE on (a) glass and (b) SiFs. Average fluorescence lifetime histogram of RPE on (c) glass and (d) SiF surface.

as the bulk-phase spectra. While recording emission spectra for different individual RPE molecules, especially on the SiF surface, we have observed significant variation of the emission maximum. These spectral changes could be a result of a number of mechanisms such as different local nanoenvironments of protein molecules on the heterogeneous silver nanostructured surface.
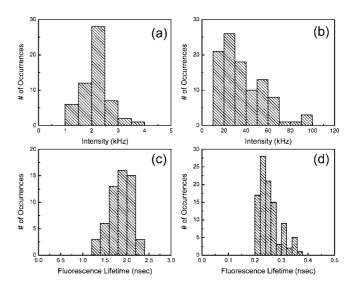
To the best of our knowledge, this is the first observation of emission spectra of individual probes on silver nanostructured surfaces.

There is a possibility of a SiF background signal in the single-molecule experiment. Silver and gold nanoparticles are known to be photoactivated with light and display characteristic "blinking" behaviors.[40,41] Strong intensity fluctuations and "nondestructive" blinking from silver nanoparticles were reported while the silver nanoparticle samples were under continuous illumination.[40,41] However the blinking behavior observed from single organic dye molecules is very different than the blinking observed from metal nanoparticles. Emission from the SiFs was not significant under our experimental conditions. Observation of the emission spectra of individual RPE molecules on SiF substrate as shown in Figure 5a further confirms that the metal-enhanced emission intensity is observed from the individual RPE molecules and not from the silver nanoparticles.

We measured the lifetimes of single RPE molecules by time-correlated single-photon counting, and the lifetimes were recovered by nonlinear least-squares. Figure 5b shows typical single-molecule intensity decays of an individual RPE molecule on glass and SiF surfaces. The average lifetime of RPE on glass is ∼2 ns. The lifetime of RPE is dramatically shortened on the SiF surface.

Panels a and b in Figure 6 show the intensity histograms of 100 RPE molecules on glass or SiF surfaces. Examination of intensity histograms for a large number of RPE molecules showed that on average the RPE molecules were more than 10-fold brighter on the SiFs than on glass. These results show that silver nanostructures can increase the brightness of RPE molecules on SiFs when compared to glass.

We measured the lifetimes of 100 RPE molecules, on glass and SiF surfaces, to determine the range of lifetimes present in each substrate. The lifetime histograms of 100 RPE molecules on glass and SiFs are shown in Figure 6c and d, respectively. These histograms (Figure 6c and d) show that the lifetimes are ∼7-fold shorter on the SiFs than on glass. The lifetime histogram

(40) Peyser, L. A.; Vinson, A. E.; Bartko, A. P.; Dickson, R. M. *Science* **2001**, *291*, 103.
(41) Geddes, C. D.; Parfenov, A.; Gryczynski, I.; Lakowicz, J. R. *J. Phys. Chem. B* **2003**, *107*, 9980.
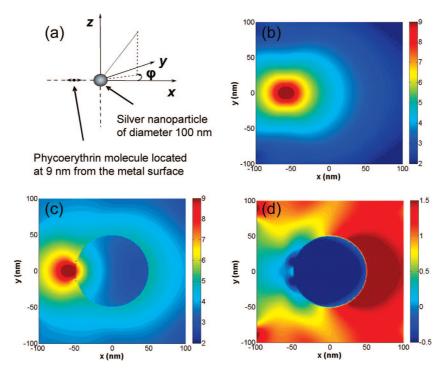
Figure 7. (a) Schematic diagram of the model radiating fluorophore/metal nanoparticle system studied using FDTD; near-field intensity distribution around (b) an isolated fluorophore oriented along the *x*-axis; (c) a 100-nm silver nanoparticle separated 9 nm from a fluorophore radiating at 570 nm; and (d) near-field enhancement around the silver particle. Note all images are displayed in the log scale.

on the SiFs does not show any of longer lifetime components comparable to that on glass. This result is consistent with the assembling of the RPE molecules on the silver nanoparticles via biotin–streptavidin chemistry and suggests high rates of excited-state RPE and silver interaction. The mean of the lifetime distribution on the SiFs is ~0.25 ns, which is much shorter than the mean on lifetime glass of ~1.8 ns. Because the molecules with the shorter lifetimes had higher intensities, these results show that the radiative decay rate of the RPE molecules is much larger on the SiFs than on glass. RPE fluorescence lifetime distributions on glass surfaces show relatively low standard deviation of ~12%, whereas the corresponding value on SiFs is ~25%. The results of Figure 6a–d show that silver nanostructures can increase the brightness and reduce the lifetime of RPE molecules on SiFs. This indicates that RPE molecules can potentially have higher photo-stability on SiFs when compared to glass.

We also examined using FDTD, the electromagnetic near-field distributions around a silver nanoparticle in the near-field of an excited fluorophore. Figure 7a is a schematic illustration of the system studied. A spherical, silver nanoparticle with a diameter of 100 nm is placed at the origin, and Φ is the azimuthal angle in the *x*–*y* plane from the *x*-axis with $0 \le \Phi < 2\pi$. The SEM images of the SiF substrates in Figure 1 revealed average particle sizes of ~100 nm, and hence, we choose this dimension for our calculations. We are aware that the morphology of the actual particles is not exactly spherical, but we choose to use the simplest shape for our calculations. The main objective of the calculations is to investigate whether an excited fluorophore in the near-field of a silver nanoparticle can cause field enhancements around the particle. We believe that any near-field enhancements induced by a fluorophore around the silver nanoparticle plays a significant role in creating the MEF that we experimentally observe. In our calculations, the fluorophore is placed 9 nm from the surface of

the silver along the negative *x*-axis. It is assumed the excitation stage of fluorescence has occurred and the fluorophore is now emitting radiation. We model this radiating fluorophore as an oscillating point dipole. The fluorophore is oriented with its dipole moment along the *x*-axis, which is perpendicular to the metal surface. Figure 7b shows the intensity around an isolated fluorophore (or oscillating dipole). We have verified that this intensity is similar to the near-field of a Hertz dipole.[37,42] Figure 7c shows the electric field intensity in the *x*–*y* plane around the 100-nm silver nanoparticle separated 9 nm from the fluorophore (oriented along the *x*-axis). Figure 7d is an image of the near-field enhancement that is generated by dividing the intensity around the fluorophore–nanoparticle complex by the intensity around the isolated fluorophore. All the images are displayed in the logarithmic scale (base 10) for clarity of presentation. The color scale for Figure 7d has been set from −0.5 to 1.5 to display regions that show both enhancement and quenching in the near-field. The areas in Figure 7d that correspond in the color map to negative values are areas where we see quenching of the near-field around the particle, and areas that correspond to positive values are areas where we see enhancements in the near-field. The locations in Figure 7d that are dark red in color and correspond in the color map to values greater than one are areas where we see maximum enhancements in the near-field around the silver particle. It is interesting to observe that the near-field is not enhanced between the particle and the dipole (deep blue in the region between the silver nanoparticle and the fluorophore), with the enhancement being distributed around the nanoparticle with the maximum on the side of the nanoparticle distal to the fluorophore (dark red in the region adjacent to the silver nanoparticle on the side opposite to the fluorophore). Such spatial variations in the near-field

(42) Shadowitz, A. *The Electromangetic Field*; Dover: New York, 1988.

enhancements are not easily inferred from experimental observations and thus provide additional insight into the nature of metal enhanced fluorescence.

In summary, our single-molecule measurements clearly show that RPE molecules display more than 10-fold increase in fluorescence intensity, with a 7-fold decrease in lifetime when they are assembled via biotin−streptavidin chemistry on silver nanostructures, as compared to control glass slides. We have also presented the ensemble measurements, which corroborate the average behavior of our single-molecule measurements. To the best of our knowledge, this is the first report demonstrating metal-enhanced fluorescence at the single-molecule level from biological macromolecules such as phycobiliproteins. The emission spectrum of individual RPE molecules displays a significant fluorescence intensity enhancement on silver nanostructures when compared to glass substrates. We believe this is the first report whereby the metal-enhanced fluorescence at the single-molecule level was measured by recording the emission spectrum from individual RPE molecules assembled separately on glass or silver nanostructured substrates. The single-molecule study provides further insight on the heterogeneity in the fluorescence enhancement and lifetimes of the RPE molecules on both glass and SiFs surfaces, which is otherwise not possible to observe using ensemble measurements. Our FDTD calculations reveal that excited-state fluorophores in the near-field of a silver nanoparticle induces enhancements of the near-fields around the silver nanoparticle.